A Method to Determine the Spatial Scale Implicated in Adhesion. Application on Human Cell Adhesion on Fractal Isotropic Rough Surfaces

Maxence Bigerelle, P. Mazeran, W. Gong, Sylvain Giljean, Karine Anselme

A Method to Determine the Spatial Scale Implicated in Adhesion. Application on Human Cell Adhesion on Fractal Isotropic Rough Surfaces

M. Bigerelle[1,3], P.-E. Mazeran[1], W. Gong[1], S. Giljean[2], and K. Anselme[2]

[1]Laboratoire Roberval, Compiègne, France
[2]Institut de Sciences des Matériaux de Mulhouse, Mulhouse, France
[3]Laboratoire TEMPO, Valenciennes, France

An extensive statistical analysis is proposed to determine the best relevant roughness parameters as a function of spatial scales that affect adhesion on surfaces. The methodology is based on a multiscale decomposition of the roughness surface and is linked with adhesion measurements. This method is applied to study cell adhesion on a very wide range of roughnesses of titanium substrates (22 surfaces, the average roughness R_a from 1 to 21 μm) tooled by an electro-erosion process and coated with a polyelectrolyte, that leads to identical surface chemistry. It is shown that the scale length of observation should be a few times the cell size to put into evidence the influence of the surface morphology on cell adhesion. It is observed that the adhesion is the lowest when the distance between the asperities of the roughness is near the cell size.

Keywords: Biomaterials; Cell adhesion; Multi-scale analyses; Osteoblastes; Roughness; Titanium

1. INTRODUCTION

Adhesion plays a major role in a large number of science and industrial fields. Adhesion between two bodies is governed by three different surfaces properties: physical and chemical properties of both surfaces and finally the roughness of the two surfaces. By selecting appropriate

surface process technologies (coating, tool-machining, etching,...), it is possible to change the surface topography without changing physical and chemical properties. Then, the influence of roughness on adhesion can be studied for a given physico-chemical surface property. In this paper, only the roughness influence on adhesion mechanisms is analyzed. The authors propose a method to determine the roughness parameters and the special scale length that are the most relevant to correlate surface topography with adhesion properties. Briefly, the method is based on a multiscale decomposition of the roughness of all samples. Then, roughness parameters are computed at all scales and the relevant roughness parameter with its associated spatial scale is chosen to best discriminate adhesion measures with topographical data.

This method is applied in the case of cell adhesion on titanium electro-eroded surfaces with different roughness (electrical discharge machining). This method has the finality to answer the global question "How does surface roughness influence adhesion?" This general question is too complex to be treated directly. This problem could be split to more specific questions on instrumental and methodological aspects:

- How to measure roughness? Which apparatus should be used? At which scale measurement should it be performed?
- How to characterize roughness? What is the most relevant roughness parameter to use?
- At which scale must the roughness parameters be evaluated?
- How is uncertainty introduced in the adhesion and roughness measurement?
- How to mathematically define the notion of influence? Is it by a mathematical function linking adhesion and roughness? If so, how to choose this function? Is it by a pure statistical modelling and, under this model, what are the required assumptions?
- How to characterize the uncertainty of this influence linking together stochastic aspects of both roughness and adhesion?

For these reasons, a methodology is developed that allows the treatment of these questions. To illustrate our purpose, this methodology is progressively treated with regard to a classical adhesion problem met in biological science: the cell adhesion on biomaterials. In this paper, the proposed methodology is treated without describing intensively the biological part.

The influence of metallic implant surface topography on the cell response has been well demonstrated over last several years using real surfaces obtained by classical surface treatment methods used for

implant surface modification (plasma-spray, sand-blasting, acid-etching) [1–7] and using model surfaces prepared by photolithography [8–12]. In order to study deeply the mechanisms of the cell response to topography, isotropic topographies over a wide range of dimensions with the same surface chemistry were tooled by electrical discharge machining (EDM). Our objective in this study was to determine if there is a sensitivity of cell adhesion to the isotropic roughness amplitude. To reach this objective, the EDM process that produces perfectly isotropic, fractal, and self-similar surfaces was used. It was shown that EDM is highly favourable for human bone cell adhesion [13,14]. Only the scale of the topography will change relatively to the cell dimensions. With this objective, 22 different samples were tooled with the EDM process, forming a very wide range of roughness overlapping the human mesenchymal stem cells length dimensions ($\sim$100 μm). Using this system, the adhesion capacity of human mesenchymal stem cells (hMSCs) can be analysed relative to the dimensions of the peaks and valleys of the topography.

The paper is organised as follows: In the first part, cell adhesion protocol, materials, and roughness measurements used to illustrate our methodology are described. Then the multiscale decomposition of roughness and roughness parameters are presented that allows description of the roughness at different scales of observation. As stochastic aspects of both adhesion and roughness are of major interest, a recent method of resampling data called the bootstrap is used. Due to intensive computation, the probability density functions of measurement of adhesion and roughness parameters are determined. Thanks to this modelling, an original statistical method based on the discriminant analyses (coupled with a Bayesian approach) is proposed to find the best roughness parameter and the scale for which adhesion is the most relevant. Finally, at this scale of relevance, an adhesion model is proposed.

2. MATERIALS AND CELL ADHESION EXPERIMENT

2.1. Preparation of Surfaces

A 5-mm thick plate of pure titanium (Ti) was electro-eroded by electrical discharge machining (EDM) using a spark erosion machine provided by Charmilles^{TM} (Meyrix, Switzerland). A copper electrode with a diameter of 20 mm was used with a tension of 220 V. Intensity and gap were controlled from 0.5 to 64 A for intensity and from 0.02 to 0.25 mm for the gap such that the first sample is the smoother and the last sample is the rougher. Then the plate was cut in order to obtain 22

samples with 22 increasing roughness grades with an amplitude roughness parameter (R_a) of between 1.2 and 21 μm (Grades 1 to 22). XPS analysis (X-Ray Spectrometer Scienta SES-200, Scienta, Courtaboeuf, France) confirmed that the surface chemistry was identical on all 22 samples (data not shown).

2.2. Roughness Measurements

2D and 3D roughness measurements were achieved on a TENCOR™ P10 tactile profilometer system using a stylus with 2-μm tip radius (KLA Tencor, Grenoble, France). The axial resolution of the machine is around 10 nm and the plane resolution is around 50 nm. As seen in Fig. 1, the surfaces obtained by electro-erosion present an isotropic structure formed by successive peaks and valleys.

No specific direction or periodical structure is visible on the surfaces. The higher the grade, the higher the roughness amplitude and the larger the peaks and valleys. The surfaces are also fractal since, when the grade rises, the surfaces appear like a zoom of the

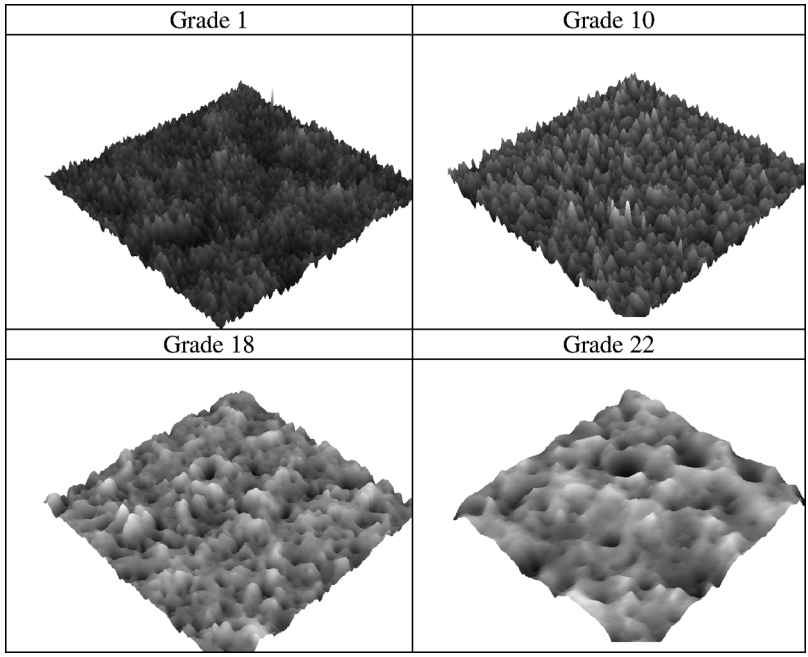

FIGURE 1 3D topographical measurements of four surfaces electro-eroded at different grades (different EDM intensities).

surface at a lower grade. A crucial point for our analysis is that the scale at which the roughness parameter influences cell adhesion is not known *a priori*. The roughness considered at either the sub-cellular scale or at the supra-cellular scale, or both, could have a strong influence. Hence, this requires that the resolution of the roughness profile starts from microns and rises to several millimetres. Another important point is that the 3D figures have a limited spatial resolution (1024×1024) that cannot really be improved, notably in the vertical direction, since 3D measures are obtained from the sum of 2D profiles taken in the horizontal direction with a shift in Y between each profile.

However, as our surfaces were perfectly isotropic (Fig. 1), the authors decided to proceed to the acquisition of 30 high-resolution 2D profiles taken randomly on each substrate to be able to develop further multiscale analysis. On each sample, 30 random profiles were measured at a 100 μm/s speed over a length of 8 mm with a 1000 Hz sampling frequency under 5 mg load. With those parameters, the distance between two consecutive points of a profile was 0.1 μm. On these profiles, roughness parameters were computed and the value for a sample was considered as the mean of 30 measurements.

2.3. Cell Cultures

Human mesenchymal stem cells (hMSCs) were prepared from the bone marrow of normal patients as previously defined [15]. hMSCs were cultured in direct contact with the surfaces during 2 hours in Iscove modified Dulbecco medium +10% fetal bovine serum + penicillin-streptomycin at 37°C in a 24-well plate. 40,000 cells were inoculated per sample. After culture, samples were rinsed in phosphate buffered saline (PBS) and fixed at least 30 minutes in paraformaldehyde 2% in NaK_2P 0.2 M buffer. After rinsing with PBS, and permeabilization with Triton® 0.2% in PBS, the cells were labelled wi1th 0.4 μg/mL FITC-phalloidin (Sigma, L'ile d'Abeau, France) and 100 ng/mL DAPI (4′,6-diamidino-2-phenylindole) (Sigma, France). The samples were observed with an epifluorescence microscope Olympus BX51 (Olympus, Rungis, France). After culture, cell layers were fixed in 2% paraformaldehyde (w/v) in qakzp 0.2 M buffer, rinsed in water, and examined in a low vacuum mode, without metallization, in an environmental scanning electron microscope at 15 kV (FEI, Lyon, France). The number of cells was determined by counting the number of nuclei labelled by DAPI on fluorescent pictures using the Image™ J 1.40 g software (Public domain software, National Institutes of Health, Bithesda, MD, USA).

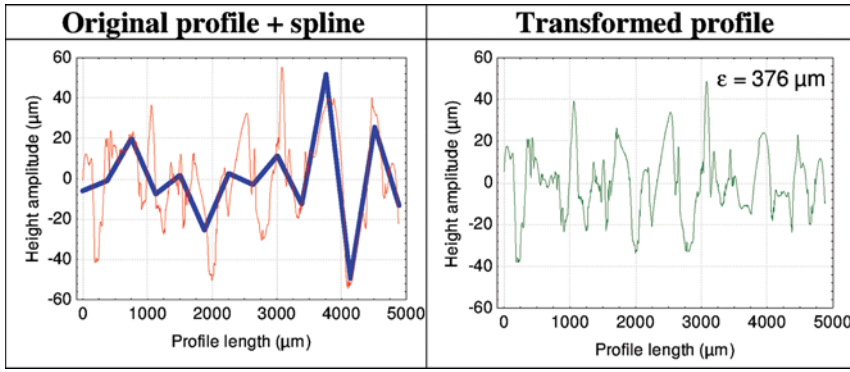

FIGURE 2 Spline decomposition of the original roughness profile of Ti sample 18 at the scale $\varepsilon = 376\,\mu m$ (right) and the transformed profile from which roughness parameters were evaluated (color figure provided online).

3. MULTI-SCALE CHARACTERISATION OF THE ROUGHNESS

As cell adhesion depends on spatial scale, a mathematical formalism was developed by the authors to analyze the profiles at different scales (see Appendix 1). This methodology was used to find:

- Form of a profile at a given scale of observation
- Residual roughness, *i.e.*, roughness when the form of the profile was removed.

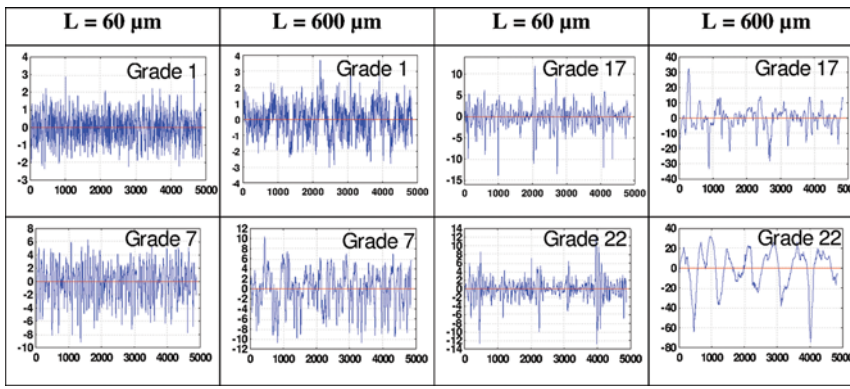

FIGURE 3 Multiscale analyses for four Grades (1, 7, 17, 22) and two scales (60 and 600 µm) (color figure provided online).

Figure 2 (left) presents the form corresponding to an evaluation length of 376 μm and the final profile (right) from which roughness parameters were estimated. Figure 3 presents the reconstructions of the same profile rectified with a first degree regression fitting corresponding to two different evaluation lengths (60 and 600 μm) for different grades of EDM. The reconstructed profiles show that the rectification for a given evaluation length corresponds to a set of high pass filters which reveal the micro-roughness.

4. ROUGHNESS PARAMETERS

4.1. Definition

Basically, surface roughness 2D parameters are normally categorized into three groups according to their functionalities. They are defined as amplitude, spacing, and hybrid parameters. These definitions are the same in 3D but another category appears corresponding to spatial parameters that can be, for example, the density of summits, the texture direction, and the dominating wavelength [16]. The more used roughness parameter in the biomaterials field is the well-known R_a parameter [17,18]. Another interesting parameter is the S_m that represents the distance between asperities on the profile. Let us consider the scheme for four cases A, B, C, and D (Fig. 4). Surfaces (A, C) have the same R_a as surfaces (B, D). On the other hand, surfaces (C, D) and surfaces (A, B) have the same S_m. This clearly means that R_a is unable to characterize lateral roughness [19] and is unable to see the skewness of the profile, *i.e.*, cannot distinguish peaks and valleys [20].

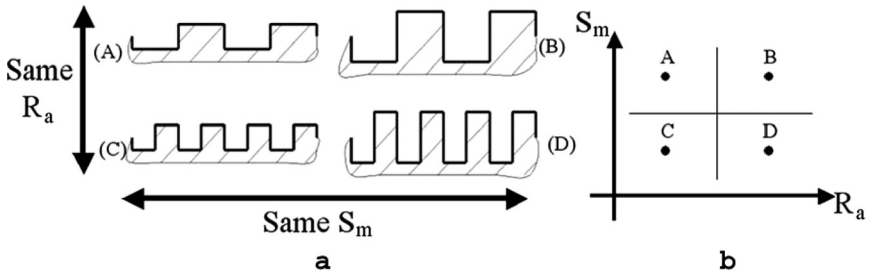

FIGURE 4 A roughness example that illustrates both S_m and R_a parameters: (a) are roughness profiles, (b) is the plot of values of S_m *versus* R_a parameters.

4.2. The Multi-Scale Roughness Parameters

Roughness parameters were calculated on all sub parts of a fixed evaluation length, ε. Then, the average value of each roughness parameter, q, noted, $q_i(\varepsilon)$, was computed by averaging on all equal parts of the profile. Thereafter, this step was reproduced for different evaluation lengths. For this investigation, the roughness profile is supposed to be ergodic, *i.e.,* roughness is homogeneous on the whole evaluation length of the profile. In this case, all multiscale measures are not spatially located and, therefore, our multiscale approach is quite different from the wavelet analysis [21–23].

Figure 5 represents the R_a and S_m parameter mean values (mean calculated from all the 30×22 profiles) *versus* the evaluation length. Each curve presents two stages: an increasing stage where the R_a or the S_m values increase with the evaluation length and an asymptotic stage where the R_a or the S_m values stay approximately constant with the evaluation length. The threshold values for ε and for R_a depend on the sample. Thus, it appears that the roughness values depend on the evaluation length and cannot be arbitrary chosen. The determination of the pertinent evaluation length is the object of the next paragraph. It must be emphasised that the log-log plot presents a linear tendency

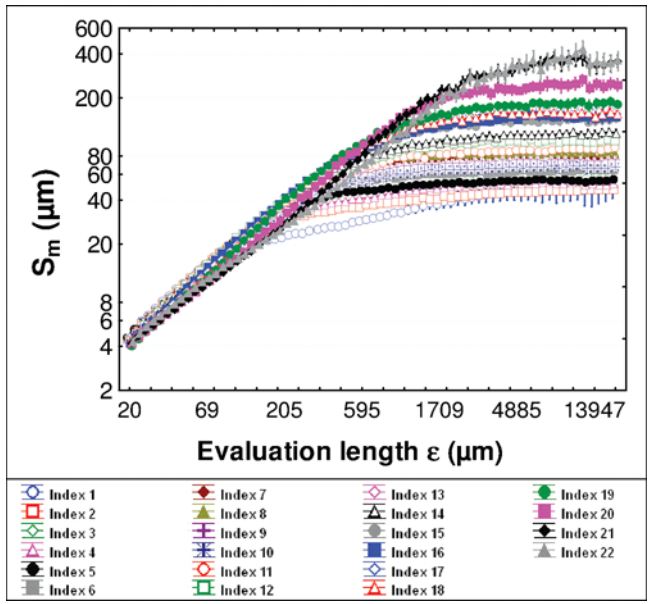

FIGURE 5 Roughness parameter values S_m *versus* the observation scale for the 22 samples (color figure provided online).

for small values of evaluation length that can be linked with the fractal dimension of the profile, Δ. For example, taking $q_i = R_t$, Tricot [24] shows that, at small evaluation lengths, the slope, H, of the log-log plot, estimates the fractal dimension of the profile ($\Delta = 2\text{-H}$). However, the linearity of the relation in a log-log graph fails in our graphs (Fig. 5), meaning that limiting the multiscale analysis only to the fractal dimension reduces the multiscale profile information. It can be noticed around 200 μm length, the relation between R_a and ε is curved downward because the profilometer tip radius (1 μm) smoothes the surface and decreases the roughness amplitude [25].

5. ADHESION AND ROUGHNESS PARAMETERS AND THEIR UNCERTAINTY

To determine the uncertainties on both adhesion measures and roughness parameters, an original statistical protocol based on the bootstrap

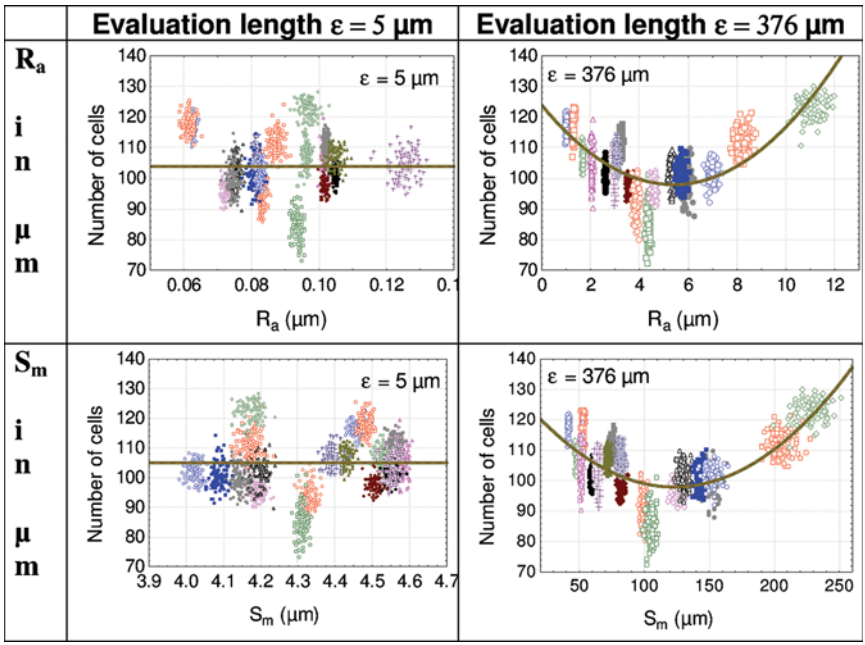

FIGURE 6 Plot of the two roughness parameters R_a and S_m at the two scales 5 μm (left) and 376 μm (right) *versus* the number of counting cells. Each point of each group (22 samples) is the mean obtained on the experimental data after resampling simulation with replacements (100 simulations by group) (color figure provided online).

theory is constructed (see Appendix 2). We process to the bootstrap simulation with two parameters $R^1 = R_a$ (the average roughness, most used parameters) and $R^2 = S_m$ (the mean distance between asperities). In this illustration, two scale analyses are used: $\varepsilon = \{5\,\mu m, 376\,\mu m\}$. 100 bootstraps (indicated by j) are then performed and $C^j_\bullet(k) = f(R^j_{a,\bullet}(5\,\mu\text{m}, k))$ for all the j bootstraps and all K surfaces (indicated by k) are plotted (Fig. 6, left bottom). Three others bootstraps were performed to plot $C^j_\bullet(k) = f(R^j_{a,\bullet}(376\,\mu\text{m}, k))$, $C^j_\bullet(k) = f(S^j_{m,\bullet}(5\,\mu\text{m}, k))$ and $C^j_\bullet(k) = f(S^j_{m,\bullet}(376\,\mu\text{m}, k))$.

Let us now briefly comment on the result of the bootstrap.

- At the scale of 5 μm, no relation seems to appear between adhesion and both roughness parameters, R_a and S_m.
- At the scale of 376 μm, a relation like a U-shape emerges between adhesion and both roughness parameters, R_a and S_m. In fact, it will be demonstrated in this paper that S_m is the best roughness parameter to characterize cell adhesion at the scale of 376 μm.
- R_a and S_m seem to follow the same law. The electro-eroded surfaces are self-affine. That means that a surface with a higher grade is identical to a surface with a lower grade if this last one is amplified by a constant factor. Indeed, if the roughness structures are the same on all grades except for a constant scale factor, the peaks and valleys will be identical except the constant scale factor and a linear relation should be found between the distance between peaks (S_m parameter) and the distance between peaks to valleys (R_t

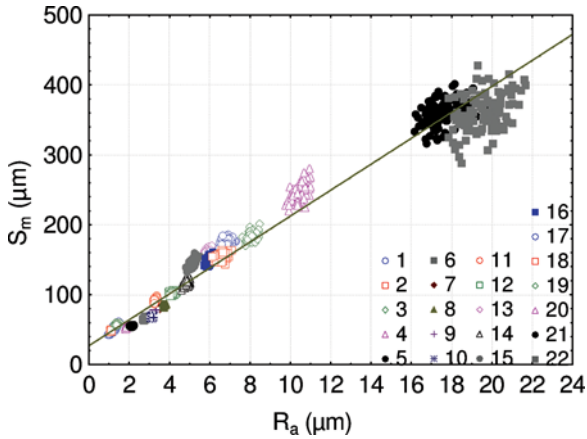

FIGURE 7 Evolution of S_m *versus* R_a for the 22 samples evaluated at the macroscopic scale (color figure provided online).

parameter, with the experimental relation $R_t \sim 8\,R_a$). This linear relation was effectively found between R_a and S_m characterized by the equation $S_m = 26.7 + 18.5 * R_a$ in μm (see Fig. 7). The good accuracy of this linear relation to fit experimental data confirms that peaks and valleys get the same shapes.

6. A METHODOLOGY TO DETERMINE THE SCALE ON WHICH ADHESION OCCURS

6.1. Problems

As shown in the previous section, at the scale of 376 μm, a relation like a U-shape emerges between adhesion and the roughness parameters R_a and S_m and no relation occurs at the scale of 5 μm. However, this analysis was only visual and limited to two scales and two roughness parameters. So the question is: "Does there exist another roughness parameter and another scale for which a better relation would emerge between adhesion and roughness characterization?" An original methodology is then created to answer this major question. A method to demonstrate mathematically what is shown in Fig. 6, *i.e.*, the S_m evaluated at the scale of 376 μm better discriminates cell adhesion than at the scale of 5 μm, must be developed. This method should be applicable for all evaluation lengths and for all roughness parameters. With this objective, an original method based on a discriminant analysis on bootstrapped data was developed (Appendix 3). This method used the discriminant analyses to determine if the data are well clustered, *i.e.*, finding the evaluation length and the roughness parameter that allow each group of samples to be better discriminated. Thanks to the use of classification functions, the number of "well classified" data for each surface was computed and one uses as a best classification indicator the mean percentage of well classified data (see Fig. 8, left). As will be illustrated in the next paragraph, this extrapolation is of major interest to find the more relevant scale and the associated roughness parameters that characterize the cell adhesion.

6.2. Results

The probability of "badly classified" data for the 81 parameters was computed for all the evaluation lengths, ε. The graph on Fig. 9 presents effectively the roughness parameters discrimination to characterize cell adhesion as a function of the scale of measurement (only three parameters are shown, R_a, S_m, and the developed surface ratio L_r). As can be observed, the best roughness parameter is obtained

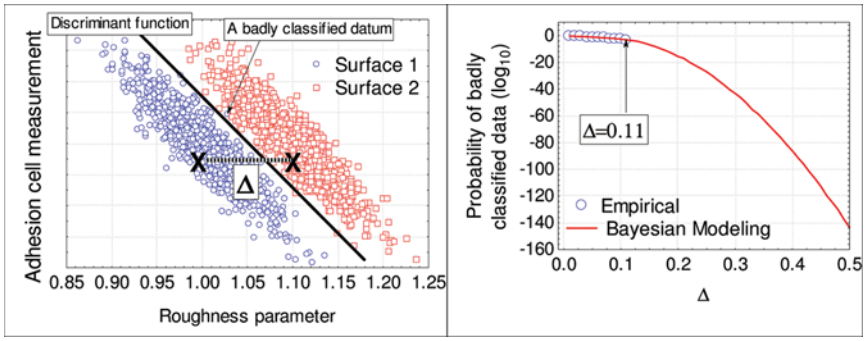

FIGURE 8 Example of discrimination between adhesion and a roughness parameter for two surfaces (left) and values of a "badly classified" datum estimated by a counting technique and a Bayesian approach (right) (color figure provided online).

for the S_m evaluation scale, $\varepsilon = 376\,\mu m$. A very important fact must be emphasized: under the size of 100 μm, the probability of badly classified data dramatically increases and this scale is around the cell size. This clearly means, thanks to this original influence graph, that below the cell size, the roughness does not influence cell adhesion. On the contrary, the L_r parameter does not influence cell adhesion at all scales. To appreciate the relevance of the discriminant analysis, the well classified data and the badly classified data are plotted for the

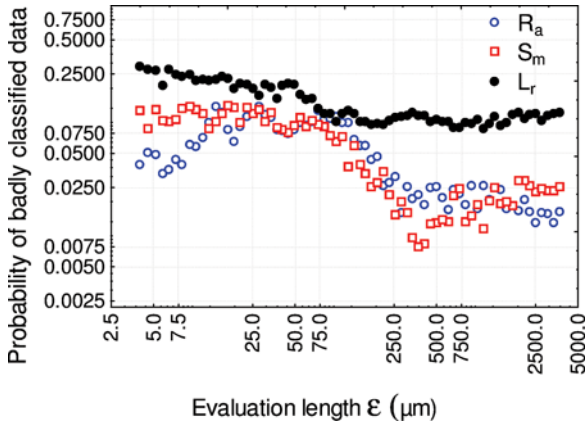

FIGURE 9 Values of the probability of "badly classified" data *versus* the evaluation length for three roughness parameters R_a, S_m, and L_r (developed surface) (color figure provided online).

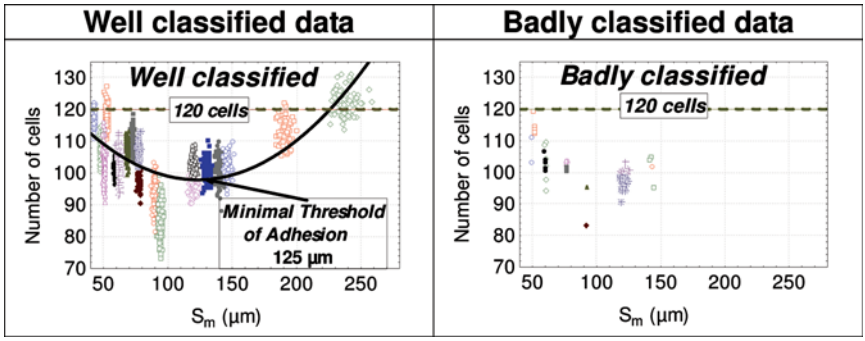

FIGURE 10 "Well classified" data (left) and "badly classified" data (right) plotted for the S_m graph presented in Fig. 5 (color figure provided online).

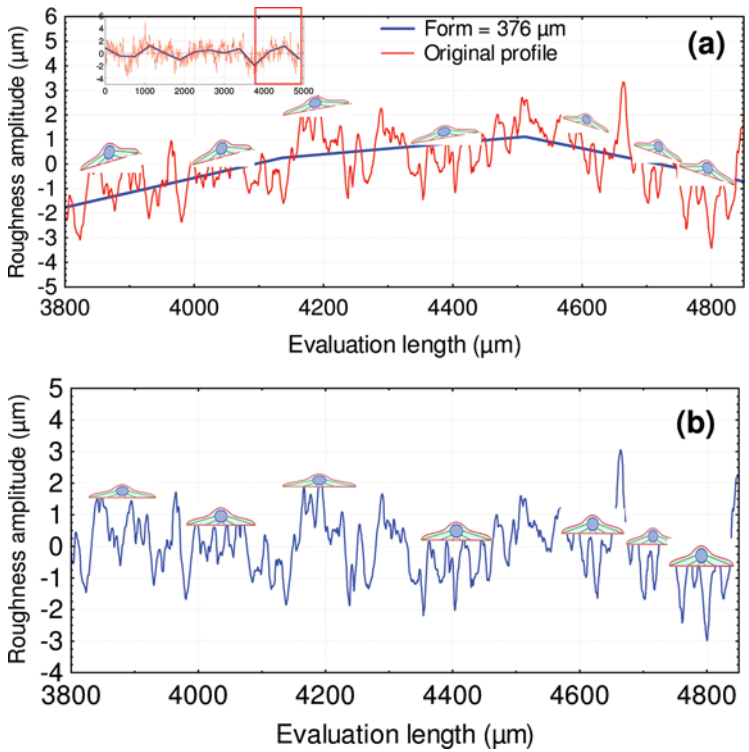

FIGURE 11 (a) Zoom of an original profile (thin line) of the surface grade 1 (see Fig. 1) and form associated with this profile obtained by the multiscale analyses at the maximal scale of relevance (376 µm). The cells are represented at their mean size value. (b) Filtering profile resulting from the form removal operation of the profile shown in (a) (color figure provided online).

S_m (Fig. 10). As can be observed, a very small number of data are badly classified (Fig. 10 on the right: amount of badly classified data is around 1%). At the more relevant evaluation scale, $\varepsilon = 376\,\mu m$, the number of cells decreases when roughness increases until, respectively, $R_a = 4\,\mu m$ and $S_m = 110\,\mu m$ (Grade 18). After this threshold, the number of cells increases with roughness until it reaches the same value as on the lowest roughness grade ($\sim$120 cells). To better visualize the effect of scale on cell adhesion, the profile of Grade 1 substrate is plotted in Fig. 11a. The function that represents the form of the surface at the scale of $\varepsilon = 376\,\mu m$ is plotted for comparison over that profile (Fig. 11a). It is clear that the variation of the profile at this scale is much larger than the cell scale. This means that cells will not see the roughness given by this form function and, thus, whatever the grade of the surface. To avoid inclusion in the future roughness analyses of these components that do not affect cell adhesion, this form will be further withdrawn from the original profile. This is illustrated in Fig. 11b that shows the profile really seen by cells

Here, a remark must be made won the graphical representation of cells on profiles and the interpretation that can be done from these figures. To visualize the roughness on the whole evaluation length, the profiles in Fig. 11 were very anamorphosed, *i.e.*, the metric scale in the roughness direction (y-axis) was very amplified compared with the scanning direction (x-axis). Then, narrow peaks appeared to be

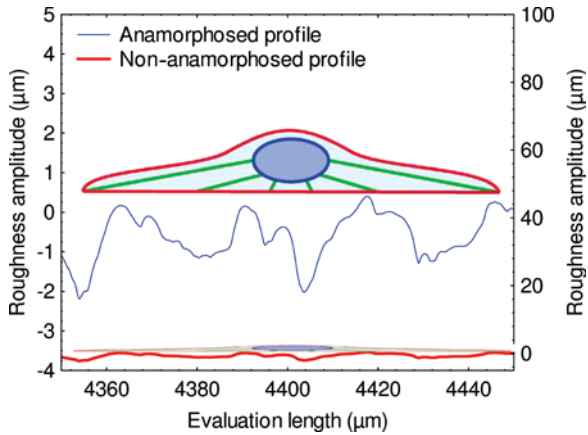

FIGURE 12 On the top, profile of Grade 1 (lower roughness) on which the cell adheres. On the bottom, the same profile at the non anamorphosed scale, *i.e.*, the vertical metric is equal to the horizontal one (color figure provided online).

present under the cells while, in reality, peaks under cells are considerably flatter (Fig. 12).

7. INTERPRETATION

7.1. Experimental Analysis

As can be observed in Fig. 10 left, the number of cells decreases significantly when S_m passes from 40 to 110 μm at the appropriate scale of observation ($\varepsilon = 376\,\mu m$). It can be stated that in an interval [$S_{m_{inf}}$, $S_{m_{sup}}$], cells are located in the valleys rather that on the peaks. In an interval [0, $S_{m_{inf}}$], they adhere rather on the top of the peaks. Then, how to explain this decrease? Roughness is stochastic in our case meaning that the morphology of peaks and valleys follows a statistical distribution, different for each grade. The lower the roughness (lower grade), the lower S_m will be. But S_m is an average, *i.e.*, it represents the mean size of the valleys (or peaks). That means that it is possible to meet some valleys (or peaks) greater than $S_{m_{inf}}$ even on samples with a mean S_m value lower that $S_{m_{inf}}$. Of course, the lower the mean S_m value, the lower the probability of meeting a peak (or a valley) wider than$S_{m_{inf}}$.

So, when the mean S_m increases, the number of peaks wider than $S_{m_{sup}}$ increases. At the scale of the cell, when peaks/valleys are greater than $S_{m_{sup}}$, peaks (and valleys) will be seen flatter and flatter and cells will only see the nanoroughness and adhere indifferently on peaks and valleys. As a consequence, cell adhesion increases as the number of peaks greater than $S_{m_{sup}}$ increases. As for cells that adhere on peaks less than $S_{m_{inf}}$, cells that adhere on peaks/valleys higher than $S_{m_{sup}}$ see the same nanoroughness (this crucial point will be demonstrated in the next section) and then it can be expected that cells on peaks/valleys $< S_{m_{inf}}$ adhere like peaks/valleys $> S_{m_{sup}}$. This leads finally to a minimal value of $S_m = 125\,\mu m$ that is near the cell size and clearly means that if peaks are around the cell size, cells do not adhere on peaks. The proposed model is summarized in Fig. 13.

7.2. Verification of the Homogeneity of the Nano-Roughness by Multiscale Analyses

In the previous section, it was claimed that cells that adhere on peaks less than $S_{m_{inf}}$ and cells that adhere on peaks/valleys higher than $S_{m_{sup}}$ see the same nanoroughness (nanoroughness represents the roughness at the scale of the solidified droplets of the EDM process).

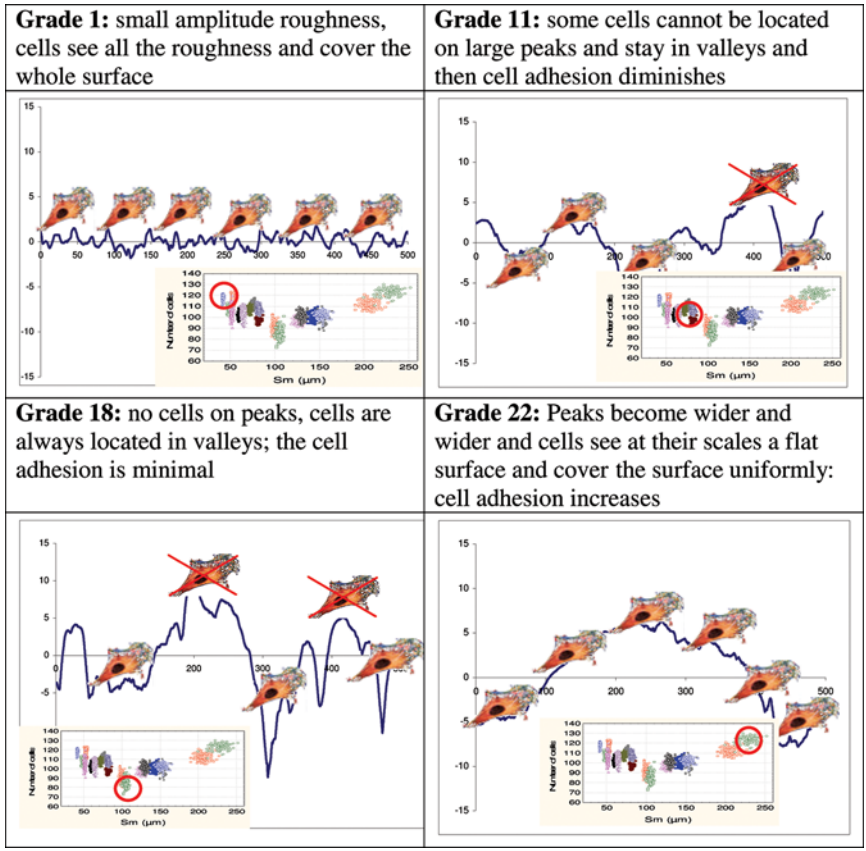

FIGURE 13 Biological explanation of the shape of graphs shown in Fig. 6 at the scale of relevance of the roughness (right) (color figure provided online).

To quantify this nano-rouhness, a wavelet analysis, that is a new and promising set of tools and techniques for analyzing the roughness signal, was used. For example, these analyses can be used in biology for cell membrane recognition to distinguish the normal from the pathological membranes. A wavelet is a waveform of effectively limited duration that has an average value of zero and is used in our case to decompose signals at a given scale. The Meyer wavelet was used to reconstruct the signal by adding all approximation components from the scale of 0.2 µm to the scale of 5 µm (about the wavelet size) (Fig. 14).

Briefly speaking, this reconstruction allows the suppression of all forms of the profile at all scales over 5 µm. Thus, the resulting profile

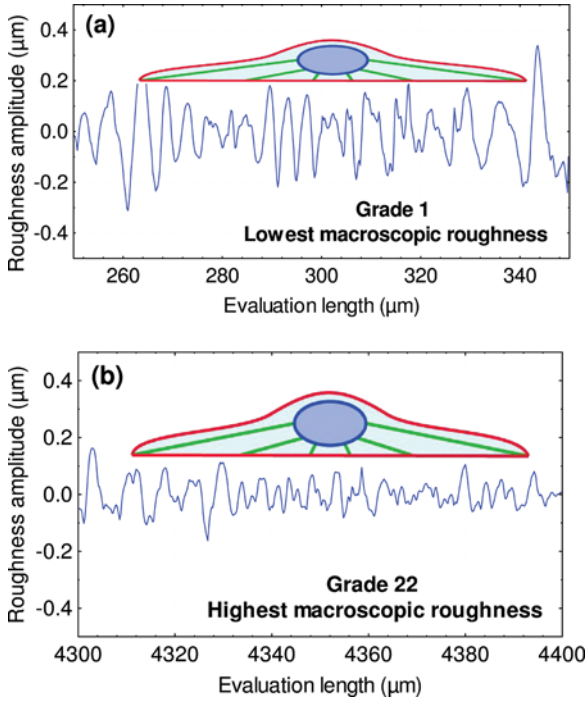

FIGURE 14 Nano roughness at the scale less than 5 μm for both (a) lowest and (b) highest roughness surface (color figure provided online).

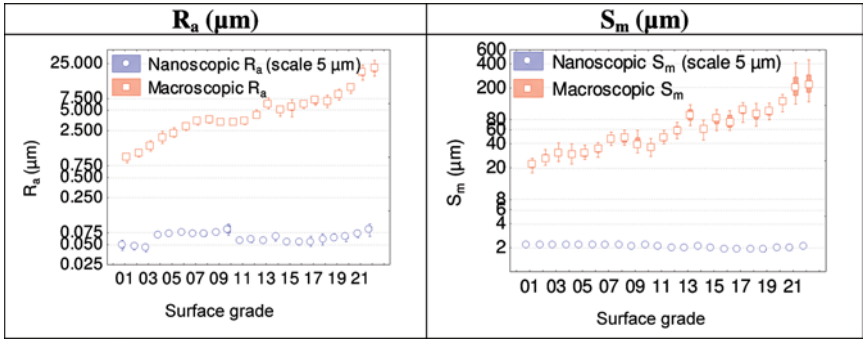

FIGURE 15 R_a and S_m reconstructed by the wavelet analysis compared with the macroscopic R_a and S_m (color figure provided online).

can be seen as a profile when all the local forms greater than 5 μm are suppressed. Then, roughness parameters are computed from these profiles. Figure 15 represents the R_a and S_m reconstructed by this wavelet analysis compared with the macroscopic R_a and S_m. As can be seen, the R_a and S_m are quite constant with grades at the 5-μm scale while they increase at the macroscopic scale. This wavelet multi-scale approach confirms the result obtained by the B-Spline function as no relation was found between S_m and cell adhesion measurement at the scale of 5 μm (Fig. 6).

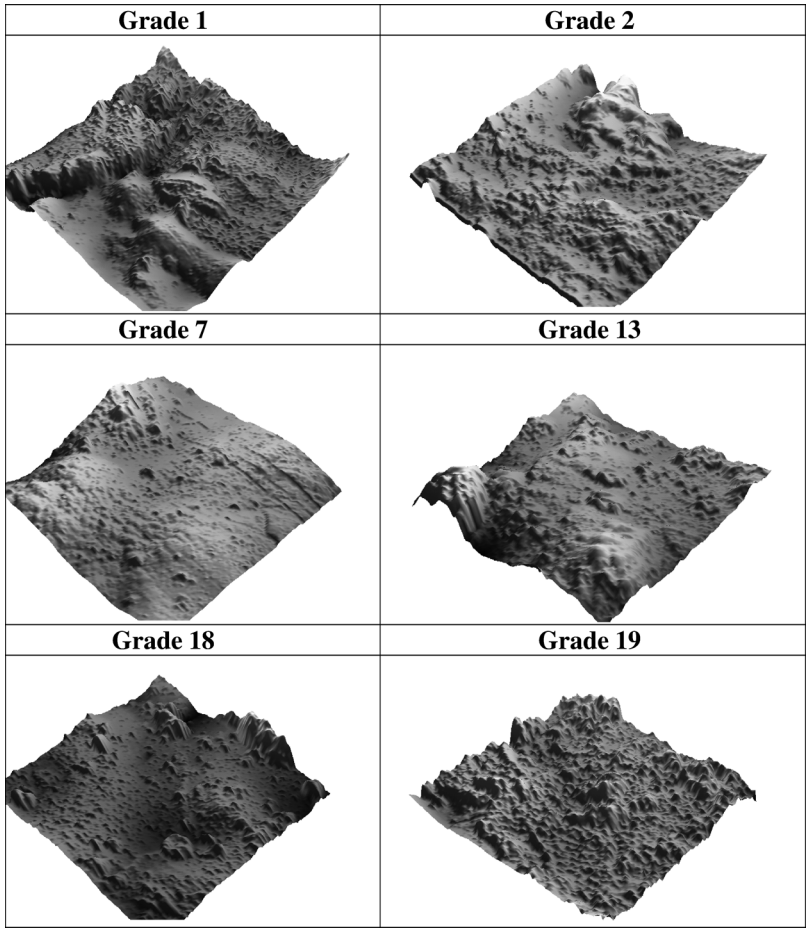

FIGURE 16 3D topographies of six samples (Grade 1, 2, 7, 13, 16, 19) obtained by AFM on a evaluation area of $5 \times 5\,\mu m^2$.

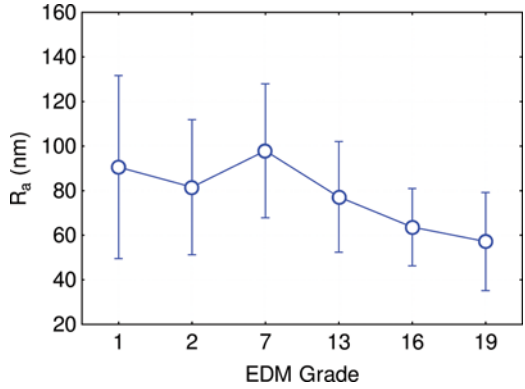

FIGURE 17 Analyses of the mean R_a (from nine measurements) of the AFM topographies described in Fig. 16 (color figure provided online).

7.3. Validation of the Multiscale Analyses by AFM Measurement

To confirm our multiscale analyses, a number of measures were carried out under atomic force microscopy (AFM). The size of the zone measured was $5 \times 5\,\mu m^2$. On each sample, nine measures were recorded on different zones. Figure 16 represents the 3D topographical maps. Thanks to an analysis of variance, R_a obtained by the nine measures taken on each sample can be considered as constant ($F = 1.56$, $p = 0.19$, see Fig. 17). As a consequence, the AFM measurement confirms the result of homogeneity of nanoroughness obtained by our multiscale analyses on a high definition profile measured by stylus profilometry.

7.4. SEM Validation of the Proposed Model of Adhesion

The SEM analysis was performed to validate the model described previously (Fig. 18). For Grade 1 (small amplitude roughness), cells see all the roughness and covered the surface. For Grade 11, some cells cannot be located on large peaks and they stay in valleys, and cell adhesion diminishes. The minimum of adhesion is given on a surface of Grade 18. At this scale, no cell is located on peaks and cells are only located in valleys of the profile and, then, the cell adhesion is lowest. When the grade increases (Grade 18→Grade 22), peaks and valleys become more and more wide and cells see at their scale a flat surface leading to an increase of cell adhesion.

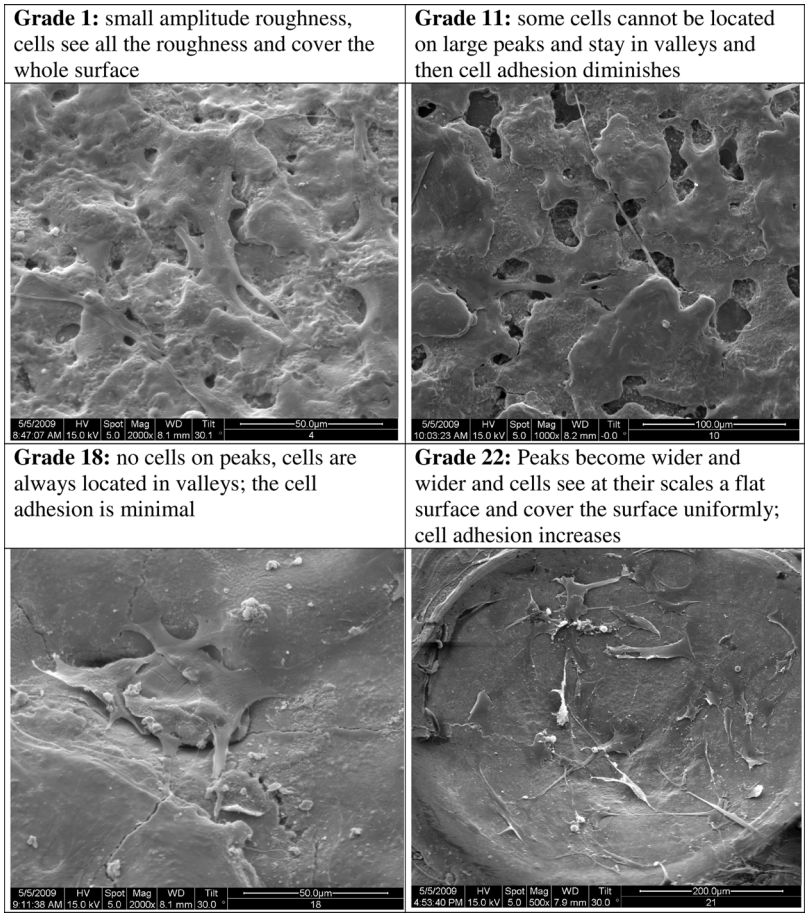

FIGURE 18 SEM photographs of osteoblastes adhesion on titanium surfaces tooled with different EDM grades.

8. CONCLUSIONS

In this paper, a new and original methodology was used to select, without preconceived opinion, relevant roughness parameters for discriminating different topographies with regard to an adhesion measure and to find at which scale adhesion is governed. Two statistical methods were combined in this methodology: the usual discriminant analysis which enabled definition and estimation of a quantitative indicator of performance (the average percentage of well classified data) for each roughness parameter and the recent and powerful computer-based

bootstrap method. This methodology was then applied to cell adhesion. Thanks to this very wide range of stochastic and self-similar roughnesses overlapping the critical dimensions of human hMSCs cells, the results of this methodology revealed that the S_m parameters measured at the scale of around 400 μm were the most relevant to be selected for discriminating the topography effect on cell adhesion. Under or over the cell size, cells see and react essentially to the nano- and sub-micron roughness that is shown to be constant for all samples.

ACKNOWLEDGMENTS

This work was also supported by the Region Picardie and the Fonds Européen de Développement Régional (FEDER) in the project "Analyse fonctionelle des surfaces rugueuses 3D."

REFERENCES

[1] Martin, J. Y., Schwartz, Z., Hummert, T. W., Schraub, D. M., Simpson, J., Lankford, J. Jr., Dean, D. D., Cochran, D. L., and Boyan, B. D., *J. Biomed. Mater. Res.* **29**, 389–401 (1995).
[2] Links, J., Boyan, B. D., Blanchard, C. R., Lohmann, C. H., Liu, Y., Cochran, D. L., Dean, D. D., and Schwartz, Z., *Biomaterials* **19**, 2219–2232 (1998).
[3] Soboyejo, W. O., Nemetsky, B., Allameh, S., Marcantonio, N., Mercer, C., and Ricci, J., *J. Biomed. Mater. Res.* **62**, 56–72 (2002).
[4] Chen, J., Mwenifumbo, S., Langhammer, C., McGovern, J. P., Li, M., Beye, A., and Soboyejo, W. O., *J. Biomed. Mater. Res. B.* **82**, 360–373 (2007).
[5] Kim, M. J., Kim, C. W., Lim, Y. J., and Heo, S. J., *J. Biomed. Mater. Res. A.* **79**, 1023–1032 (2006).
[6] Ball, M., Grant, D. M., Lo, W. J., and Scotchford, C. A., *J. Biomed. Mater. Res. A.* **86**, 637–647 (2008).
[7] Le Guehennec, L., Soueidan, A., Layrolle, P., and Amouriq, Y., *Dent. Mater.* **23**, 844–854 (2007).
[8] Zinger, O., Anselme, K., Denzer, A., Habersetzer, P., Wieland, M., Jeanfils, J., Hardouin, P., and Landolt, D., *Biomaterials* **25**, 2695–2711 (2004).
[9] Ismail, F. S. M., Rohanizadeh, R., Atwa, S., Mason, R. S., Ruys, A. J., Martin, P. J., and Bendavid, A., *J. Mater. Sci.- Mater. Med.* **18**, 705–714 (2007).
[10] Lu, J., Rao, M. P., MacDonald, N. C., Khang, D., and Webster, T. J., *Acta Biomater.* **4**, 192–201 (2008).
[11] Khang, D., Lu, J., Yao, C., Haberstroh, K. M., and Webster, T. J., *Biomaterials* **29**, 970–983 (2008).
[12] Matschegewski, C., Staehlke, S., Loeffler, R., Lange, R., Chai, F., Kern, D. P., Beck, U., and Nebe, B. J., *Biomaterials* **31**, 5729–5740 (2010).
[13] Anselme, K. and Bigerelle, M., *Acta Biomater.* **1**, 211–222 (2005).
[14] Anselme, K. and Bigerelle, M., *Biomaterials* **27**, 1187–1199 (2006).
[15] Anselme, K., Broux, O., Noël, B., Bouxin, B., Bascoulergue, G., Dudermel, A. F., Bianchi, F., Jeanfils, J., and Hardouin, P., *Tissue Eng.* **8**, 941–953 (2002).

[16] Stout, K. J., Sullivan, P. J., Dong, W. P., Mainsah, E., Luo, N., Mathia, T., Sullivan, P. J., and Zahouani, H., *Development of Methods for the Characterization of Roughness in Three Dimensions*, (Penton Press, London, 2000).
[17] ASME Y14.36 M-1996 *Surface Texture Symbols*, (American Society of Mechanical Engineers, 1996).
[18] ISO 1302:2002 *Geometrical Product Specifications (GPS) – Indication of Surface Texture in Technical Product Documentation*, (2002).
[19] AS ISO 1302–2005 *Geometrical Product Specifications (GPS) – Indication of Surface Texture in Technical Product Documentation*, (2005).
[20] Bigerelle, M. and Iost, A., *Tribol. Int.* **40**, 1319–1334 (2007).
[21] Niola, V., Nasti, G., and Quaremba, G., *J. Mater. Process. Technol.* **164**, 1410–1415 (2005).
[22] Wang, A. L., Yang, C. X., and Yuan, X. G., *Tribol. Int.* **36**, 527–535 (2003).
[23] Josso, B., Burton, D. R., and Lalor, M. J., *Comput. Method. Appl. M.* **191**, 829–842 (2001).
[24] Tricot, C., *Compos. Sci. Technol.* **63**, 1089–1096 (2003).
[25] Bigerelle, M., Najjar, D., and Iost, A., *Wear* **258**, 232–239 (2005).
[26] Farin, G., *Curves and surfaces for Computer-Aided Geometric Design: A Pratical Guide*, 4th ed., (Academic press, San Diego, CA, 1996).
[27] Efron, B., *Ann. Stat.* **7**, 1–26 (1979).
[28] Efron, B. and Tibshirani, R., *Stat. Sci.* **1**, 54–77 (1986).
[29] Efron, B. and Tibshirani, R., *Science* **253**, 390–395 (1991).
[30] Efron, B. and Tibshirani, R., *An Introduction to the Bootstrap*, (Chapman and Hall/CRC, Boca Raton, FL, 1993).
[31] Najjar, D., Bigerelle, M., and Iost, A., *Wear* **254**, 450–460 (2003).
[32] Fisher, R. A., *Annals of Eugenics.* **7**, 179–188 (1936).
[33] Cooley, W. W. and Lohnes, P. R., *Multivariate Data Analysis*, (John Wiley and Sons, New York, 1971).
[34] [34 Tatsuoka, M. M., *Multivariate Analysis*, (John Wiley and Sons, New York, 1971).
[35] Kshirsagar, A. M., *Multivariate Analysis*, (Marcel Dekker, New York, 1972).
[36] Lachenbruch, P. A., *Discriminant Analysis*, (Hafner, New York, 1975).
[37] Lachenbruch, P. A., *Biometrics* **35**, 69–85 (1979).
[38] Gnanadesikan, R., *Methods for Statistical Data Analysis of Multivariate Observations*, (John Wiley and Sons, New York, 1979).
[39] Klecka, W. R., *Sage University paper series on quantitative application in the social sciences*, (Sage Publications Beverly Hills, CA, USA 1980), pp. 72, 07-019.
[40] Hand, D. J., *Discrimination and Classification*, (John Wiley and Sons, New York, 1981).
[41] Hand, D. J., *Kernel Discriminant Analysis*, (Research Studies Press, New York, 1982).
[42] Glick, N., *Pattern. Recogn.* **10**, 211–222 (1978).
[43] Hora, S. C. and Wilcox, J. B., *J. Marketing. Res.* **19**, 57–61 (1982).

APPENDIX 1: THE MULTISCALE ANALYSES OF ROUGHNESS

In this part, a mathematical formalism is developed to analyze the profiles at different scales. Each experimental profile is split into equal parts of a given length and each part of the profile will be considered

as a new profile. Consecutively, the horizontal length of these profiles will be considered as the evaluation length. To delete "the shape" greater than the evaluation length, each profile part was rectified by a d-degree polynomial least squares fitting using continuous regression. To remove the local forms, the regression parameters were computed on a given window by imposing a C^{d-1} continuity between adjacent polynomials defined on the two neighbour windows ($d = 1$ in this paper). As a consequence, the form profile is a B-spline function [26] described by a parametric representation which minimises the quadratic distance with regard to the profile [26]. The equation defined by the B-spline induces a more realistic representation of the profile form without including artificial roughness.

The B-spline is defined as follows:

Let a B-spline function be described by the parametric representation $\mathbf{B}(t) = \begin{vmatrix} X(t) \\ Y(t) \end{vmatrix}$ which minimises the quadratic distance with regard to the profile. This B-spline is defined by a list of control points $\{\mathbf{P_0}, \mathbf{P_1}, \ldots, \mathbf{P_K}\}$ whose number K corresponds to the number of windows along the scanning length and the associated knot sequence $\{u_0, u_1, \ldots, u_K\}$. More precisely, a B-spline can be written as follows: $\mathbf{B}_{d,K}(t) = \sum_{i=0}^{K} \mathbf{P_i} \cdot N_{i,d}(t)$ where $\mathbf{P_i} = \begin{vmatrix} X_i \\ Y_i \end{vmatrix}$ are the control points and $N_{i,\,d}$ is the polynomial function with degree d defined by the recursive scheme:

$$N_{i,n}(t) = \frac{t - u_{i-1}}{u_{i+n-1} - u_{i-1}} N_{i,n-1}(t) + \frac{u_{i+n} - t}{u_{i+n} - u_i} N_{i+1,n-1}(t) \quad \text{with } N_{i,0}(t) = \begin{cases} 1 & \text{if } t \in [u_{i-1}, u_i] \\ 0 & \text{else} \end{cases}. \tag{1}$$

To simplify the problem, we have taken $X(t) = t$ and the fitting problem becomes a minimisation of the quadratic distance

$$\sum_{i=0}^{L} \|y_i - Y(x_i)\|^2 \tag{2}$$

with $\begin{vmatrix} x_i \\ y_i \end{vmatrix}$ the coordinates of the points of the profile and L their number,that corresponds to:

$$\sum_{i=0}^{L} \left[y_i - \sum_{j=0}^{K} Y_j \cdot N_{j,n}(x_i) \right] N_{Q,n}(x_i) = 0 \quad \forall Q \in \{0, \ldots, K\} \tag{3}$$

or

$$\overrightarrow{\mathbf{Y}} = \overline{\overline{\mathbf{M}}} \cdot \overrightarrow{\mathbf{P}} = \begin{vmatrix} \sum_{i=0}^{L} y_i \cdot N_{0,n}(x_i) \\ \vdots \\ \sum_{i=0}^{L} y_i \cdot N_{Q,n}(x_i) \\ \vdots \\ \sum_{i=0}^{L} y_i \cdot N_{K,n}(x_i) \end{vmatrix} \quad \text{with } \overrightarrow{\mathbf{P}} = \begin{vmatrix} Y_0 \\ \vdots \\ Y_Q \\ \vdots \\ Y_K \end{vmatrix}, \tag{4}$$

with:

$$\overline{\overline{\mathbf{M}}} = (m_{j,k}) \text{ and } m_{j,k} = \sum_{i=0}^{p} N_{j,n}(x_i) \cdot N_{k,n}(x_i). \tag{5}$$

Using Eqs. (1–5) vector $\overrightarrow{\mathbf{P}} = \left(\overline{\overline{\mathbf{M}}}\right)^{-1} \cdot \overrightarrow{\mathbf{Y}}$ is obtained. After the B-spline curve calculation, the profile is rectified by subtracting the B-spline.

APPENDIX 2: BOOTSTRAP ESTIMATION OF UNCERTAINTY BETWEEN ADHESION AND ROUGHNESS PARAMETERS

In this part, a method is developed to determine the uncertainties of both adhesion measurements and roughness parameters. One gets K = 22 samples with $k \in \{1, 2, \ldots, K\}$. On each sample, P measures with $p \in \{1, 2, \ldots, P\}$ of cells counting noted $C_p(k)$ were processed. In another way, N roughness measures with $n \in \{1, 2, \ldots, N\}$ evaluated at the scale ε were processed on each sample from which R roughness parameters with $r \in \{1, 2, \ldots, R\}$ and noted R^r were computed. Finally $R_n^r(\varepsilon, k)$ represents the roughness parameters R^r (for example $R^1 = R_1$) evaluated at the scale ε and computed from the nth roughness measurement of the kth surface. However, no correlation exists between $R_n^r(\varepsilon, k)$ and $C_p(k)$ for given k and ε. So it becomes necessary to compute means $R_n^r(\varepsilon, k)$ noted $R_\bullet^r(\varepsilon, k)$ for each k and ε and means of $C_p(k)$ noted $C_\bullet(k)$ for each k surfaces. At this step, $R_\bullet^r(\varepsilon, k)$ are plotted *versus* $C_\bullet(k)$ for each scale ε and a possible relation between the roughness parameters $R_\bullet^r(\varepsilon, k)$ and the cell adhesion $C_\bullet(k)$ for a given scale ε can be observed. However, a major criticism is that the uncertainty of the data are lost. It is a major interest to construct the bivariate probability density function of $(R_\bullet^r(\varepsilon, k), C_\bullet(\mathrm{k}))$ for all k samples at a given scale ε. As the form of probability density function is not known *a priori*, a rough assumption could be done as a Gaussian hypothesis.

To avoid this classical way of analyses, a recent statistical method was created and is called the bootstrap. Bootstrap theory was first introduced by Efron [27–30]. Roughly speaking, this computer-based bootstrap method (CBBM), which is described in this paper, allows the replacement of statistical inference assumptions (therefore limiting the risk to assert wrong conclusions) by intensive calculations while making the most of the power of modern personal computers. The efficiency of the proposed methodology is emphasised in this work through the study of the relationships between the cell adhesion level and the surface roughness of coated titanium biomaterials. The main principle of our bootstrap protocol CBBM consists in generating a high number K ($=100$ in this study) of simulated bootstrap samples from the experimental data points exploiting the power of a modern computer. A bootstrap sample of size n, referred to by k ($1 \leq k \leq K$) and noted $(t_1^k, t_2^k, \ldots, t_n^k)$, is a collection of n values obtained by randomly sampling with replacement from the experimental data points $(t_1^{Exp.}, t_2^{Exp.}, \ldots, t_n^{Exp.})$. The bootstrap data set, thus, consists of some elements of the original data set: some never appearing, others appearing once, others appearing twice, etc. Whatever the sample k in which the measurements have been carried out, the experimental data set contains P values $\{C_1^{Exp.}(k), C_2^{Exp.}(k), \ldots, C_P^{Exp.}(k)\}$ of cell adhesion measurements and N values $\{R_1^{r,Exp.}(k,\varepsilon), R_2^{r,Exp.}(k,\varepsilon), \ldots, R_N^{r,Exp.}(k,\varepsilon)\}$ of the roughness parameter R^r under consideration. The simulated bootstrap samples obtained by randomly sampling with replacement scores of the experimental data set, are, respectively, noted $\{C_1^j(k), C_2^j(k), \ldots, C_P^j(k)\}$ and $\{R_1^{r,j}(k,\varepsilon), R_2^{r,j}(k,\varepsilon), \ldots, R_N^{r,j}(k,\varepsilon)\}$; the superscript j refers to the jth bootstrap simulation. The means of these newly simulated samples were then calculated for each grade k and are, respectively, noted $R_\bullet^{r,j}(\varepsilon,k), C_\bullet^j(k)$. These means were reported on a graph $C_\bullet^j(k) = f(R_\bullet^{r,j}(\varepsilon,k))$ for all the $\mathrm{J}=100$ bootstraps and the $\mathrm{K}=22$ surfaces and, thus, at a given scale ε.

APPENDIX 3: ORIGINAL METHOD FOR THE CLASSIFICATION OF THE ROUGHNESS PARAMETER WITH ITS APPROPRIATE SCALE

For each evaluation length and each sample, 81 different roughness parameters were computed (spectral, autocorrelation, fractal, amplitude, peaks, hybrid, morphological, etc.). Actually, the evaluation length at which the parameter is computed must be chosen according to the surface functionality tested. In our case, the functionality of the surface was its ability to increase cell adhesion properties and, more

specifically, the number of cells adhered on the surface after 2 days. However, some problems remain before performing a statistical correlation analysis. Firstly, variation exists in both quantifications of attached cells and roughness measurements, these variations being not related. Secondly, the mathematical relation between roughness and cell response is unknown. Finally, one should find a method that allows defining the roughness parameter that, at a specific evaluation length ε, better discriminates between the different grades and their functionalities. More precisely, our objective is to find a method that determines if the data are well clustered, *i.e.*, finding the evaluation length and the roughness parameter that allow each group of samples to be better discriminated. The main problems are now to find a statistical method to treat the cited problems, *i.e.*, the best roughness parameter and its associated scale that allows us to discriminate adhesion. The factorial method called *discriminant analyses* will be used as the statistical tool to answer the cited problem [32–41]. Discriminant function analysis was used to determine which variables to discriminate between two or more naturally occurring groups. The basic idea underlying discriminant function analysis is to determine whether groups differ with regard to the mean of a variable, and then to use that variable to predict group membership.

Thanks to the power of actual computers, an original method is proposed to give some visual indicators or relevancy. The basic idea is to process a discriminant analysis for all the roughness parameters at all scales. For each of the p pairs of parameters (*adhesion, roughness parameter with its own scale*), thanks to the use classification functions, the number of well classified data in each class (class = surface)) indicated by c_k was computed and noted as $n_w(q_j(\varepsilon),c_k)$. On the other hand, $n_b(q_j(\varepsilon),c_k)$ denoted the number of badly classified with $n(q_j(\varepsilon), c_k) = n_w(q_j(\varepsilon),\ c_k) + n_b(q_j(\varepsilon),\ c_k)$. $n(q_j(\varepsilon),c_k,c_l)$ denotes the number of classified data that originally belong to the class c_k and were classified in the c_l classes with $n_w(q_j(\varepsilon),\ c_k) = n(q_j(\varepsilon),c_k,c_k)$ and $n_b(q_j(\varepsilon), c_k) = \sum_{\substack{l\in Nc \\ l\neq k}} n(q_j(\varepsilon), c_k, c_l)$ where Nc is the number of classes. Then, one uses as a best classification indicator noted $p_w(q_j(\varepsilon))$ the mean percentage of well classified data:

$$p_w(q_j(\varepsilon)) = 100/Nc \sum_{k\in Nc} \left(n(q_j(\varepsilon), c_k, c_k) / \sum_{l\in Nc} n(q_j(\varepsilon), c_k, c_l) \right). \qquad (1)$$

and $p_b(q_j(\varepsilon))$ the mean percentage of badly classified data:

$$p_b(q_j(\varepsilon)) = 100 - p_w(q_j(\varepsilon)). \qquad (2)$$

However, the proposed methodology possesses a limit because the relevancy of a roughness parameter is based on the empirical counting of the percentage of well classified data in the c_k class. The two parameters $q_i(\varepsilon_{i'})$ and $q_j(\varepsilon_{j'})$ can discriminate 100% of experimental data (meaning that percentage of badly classified data is equal to 0%). In this case, it becomes difficult to quantify if the $q_i(\varepsilon_{i'})$ parameter is better than $q_j(\varepsilon_{j'})$ if both these parameters classified data without any error (0% of badly classified data). To illustrate this purpose, the case of only two surfaces was analyzed. Figure 8 represents the plot of adhesion value *versus* an arbitrary roughness parameter value. The linear discriminate function splits the two groups and it can be observed that some data are classified as bad. The symbol Δ denotes the distance between the two gravity centers of each group. The higher Δ is, the higher the roughness parameter discriminates adhesion. However, over a critical value of Δ, 100% of data are well classified and then it becomes impossible to claim if a roughness parameter better discriminates adhesion than another one if both allow the classification of 100% of data. As a consequence, the density probability function of the group has to be interpolated to formulate a probability of badly classified (or well classified) data. More precisely, we use a Bayesian approach to compute the probability error-rate estimates for each group [42, 43]. Figure 8 (right) represents the value of the theoretical probability and the empirical one. As can be observed, at a pass over threshold of $\Delta = 0.11$, all data are well classified and our Bayesian approach allows us to extrapolate the probability of badly classified data.